Phase diagram of ferroelectric $BaTiO_3$ ultrathin films under open-circuit conditions

2008 J. Phys.: Condens. Matter 20 135203

(http://iopscience.iop.org/0953-8984/20/13/135203)

J. Phys.: Condens. Matter **20** (2008) 135203 (6pp) doi:10.1088/0953-8984/20/13/135203

Phase diagram of ferroelectric $BaTiO_3$ ultrathin films under open-circuit conditions

Jie Yu[1], **Zhongqing Wu**[1], **Zhirong Liu**[2], **Qimin Yan**[1], **Jian Wu**[1] and **Wenhui Duan**[1,3]

[1] Department of Physics, Tsinghua University, Beijing 100084, People's Republic of China
[2] College of Chemistry and Molecular Engineering, Peking University, Beijing 100871, People's Republic of China

E-mail: dwh@phys.tsinghua.edu.cn

Received 15 June 2007, in final form 14 February 2008
Published 7 March 2008
Online at stacks.iop.org/JPhysCM/20/135203

Abstract

Using a first-principles-based Monte Carlo approach, we investigate the strain–temperature phase diagram of $BaTiO_3$ ultrathin film without any surface charge screening. Although the depolarizing field has little effect on the phase types, a unique stripe domain structure with periodic out-of-plane polarization forms in the ultrathin films to minimize the energy of the depolarizing field under the constraint of the boundary condition, which leads to an unusual characteristic of the phase diagram. As a result, the total out-of-plane polarization remains zero at any strain and temperature. The film thickness has obvious effects on the phase diagram, e.g. the Curie temperature decreases and the strain moves to more negative values when the film thickness decreases. It is found that the compressive strain plays a decisive role in the characterization of ferroelectric polarization in such films, which suppresses the in-plane polarization while supporting the out-of-plane polarization, and thus drives the polarization to rotate from the in-plane to the normal direction.

(Some figures in this article are in colour only in the electronic version)

Thin films have extraordinary properties that are different from the bulk material [1–3]. Along with the improvement of bottom-up experimental techniques, ferroelectric films [4] and superlattices [5] have been scaled down to nanometer size with thicknesses of only a few unit cells. Barium titanate ($BaTiO_3$) thin films have been extensively studied due to their promising ferroelectric properties and various possible applications from the computer industry to medical use [6–8]. Recently, ferroelectric characteristics were experimentally observed in a $PbTiO_3$ film only three unit cells thick [4] and a very high transition temperature was found in the ferroelectric $BaTiO_3$ superlattice [9]. More and more experimental evidence supports the opinion that it is the strain from the mismatch between the film and substrate that induces a dramatic increase in the phase transition temperatures [10]. The experimental advances offered a great theoretical challenge to explore the inherent physics of ferroelectric properties in nanoscale ultrathin film by imposing strain and temperature effects. The strain–temperature phase diagram for epitaxial and single domain [001] $BaTiO_3$ thin films has been predicted using the Landau–Ginzburg–Devonshire (LGD) thermodynamic theory [11] and first-principles based simulation [12] with periodic boundary conditions. The effects of film thickness, surface, and electric field were recently addressed by Lai *et al* [13, 14]. All these works assumed ideal short-circuit (SC) electrical conditions or near-SC conditions. However, real thin films probably exhibit a depolarizing field [15], which may limit the functional performance of the device [16]. In fact, the residual depolarizing field would result in a rich variety of ferroelectric phases and polarization patterns [17, 18]. Under the extreme conditions of ideal open-circuit conditions, some unusual behaviors, such as the off-center displacement vortex pattern in $BaTiO_3$ quantum dots [19], vortex stripes in $Pb(Zr_{0.5}Ti_{0.5})O_3$ (PZT) [17, 20], and a polarization antiparallel to the external field [20, 21], have been revealed. The aim

[3] Author to whom any correspondence should be addressed.

of this work is to theoretically explore the phase diagram and the polarization patterns of $BaTiO_3$ ultrathin films under open-circuit conditions.

There are diverse approaches to investigate perovskite ferroelectrics [22, 23]. We adopt the first-principles-based effective Hamiltonian scheme [24, 25]. In this approach, an effective Hamiltonian is derived from first-principles calculations by expanding the total energy around the paraelectric structure with respect to relevant variables: soft mode and strain (since atomic displacements and strain deformations induced by ferroelectric phase transition are relatively small). Then the effective Hamiltonian can be used in Monte Carlo simulations to investigate the properties of the system under various conditions. The approach has been widely applied to many ferroelectrics [13, 18–20, 24–29]. For $BaTiO_3$, the total energy E is written as the sum of a local mode self-energy, a long-range dipole–dipole interaction, a short-range interaction between soft modes, an elastic energy, and an interaction between the local modes and local strain energy, as follows [24]:

$$E^{\mathrm{tot}}(\{\mathbf{u}_i\},\{\mathbf{v}_i\},\{\eta_{\mathrm{H}}\}) = E^{\mathrm{self}}(\{\mathbf{u}_i\}) + E^{\mathrm{dpl}}(\{\mathbf{u}_i\}) + E^{\mathrm{short}}(\{\mathbf{u}_i\}) + E^{\mathrm{elas}}(\{\eta_{\mathrm{H}}\},\{\mathbf{v}_i\}) + E^{\mathrm{int}}(\{\mathbf{u}_i\},\{\mathbf{v}_i\},\{\eta_{\mathrm{H}}\}), \quad (1)$$

where $\mathbf{u}_i$ is the local soft mode in the ith unit cell which is related to electrical dipoles P_i via $P_i = Z^*\mathbf{u}_i$ (Z^* is the effective charge of the local mode), $\mathbf{v}_i$ is the dimensionless local displacement related to the inhomogeneous strain, and η_{H} is the homogeneous strain tensor. All parameters are determined from first-principles calculations with the local density approximation (LDA) under zero temperature. The detailed expression and the parameters of the Hamiltonian were listed in [24].

The $BaTiO_3$ thin films under our consideration are grown along the [001] direction (denoted as the z-axis thereafter) with N_z cell layers. The x- and y-axes are chosen to be along the pseudocubic [100] and [010] directions, respectively, where periodic boundary conditions are applied inside the films with $N_x \times N_y$ cells. Obviously, the film thickness is $N_z \times a$, where $a = 3.94$ Å is the lattice constant of the bulk $BaTiO_3$. The influence of the substrate is imposed by confining the homogeneous in-plane strain, i.e. $\eta_1 = \eta_2 = \eta$ and $\eta_6 = 0$ (in the Voigt notation). The vacuum surrounding the thin films is expected to cause surface induced relaxations. The surface effect is implicitly accounted for in our simulations by (i) including the effect of the broken bonds in the surfaces, which is substantial for the surface energy; and by (ii) relaxing all the local soft modes and inhomogeneous strains under the effective Hamiltonian with the thin film geometry. The external term of the surface effect is not included in the Hamiltonian since the term has almost no effect on the polarization pattern [18, 19]. Open-circuit conditions are used here, so the effect of depolarization field is considered without any surface charge screening.

The equilibrium properties of $BaTiO_3$ thin films under various conditions (temperature, strain, film thickness, etc) are determined by use of Monte Carlo simulations based on the effective Hamiltonian equation (1). The Metropolis algorithm

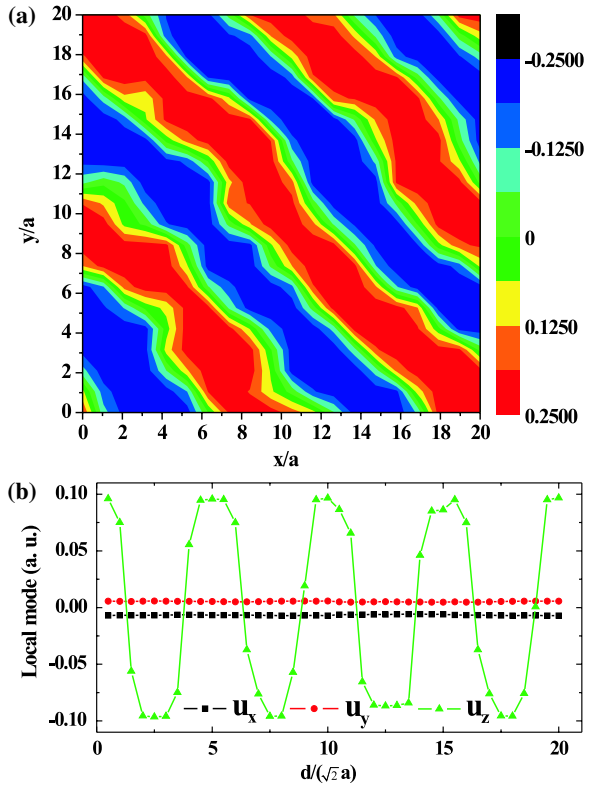

Figure 1. (a) The domain structure in the x–y plane of the film under a compressive strain. The supercell we chose is $20 \times 20 \times 8$, the simulation temperature is 160 K, and the strain imposed on the film is -0.4%. The color bar represents the magnitude of the out-of-plane polarization (u_z). (b) The plane average of the local soft mode (u_x, u_y, and u_z) for the supercell along the (110) direction.

is adopted in our simulation on a $N_x \times N_y \times N_z$ supercell lattice. The corrected three-dimensional Ewald method [30] is adopted to speed up the calculation of the long-range dipole–dipole interaction energy. The single-flip move is chosen. In one Monte Carlo sweep (MCS), we first make a trail move on each $\mathbf{u}_i$ in sequence, then each $\mathbf{v}_i$ in sequence, and then repeat this several times on the homogeneous strain variables. The step sizes are adjusted to ensure an acceptance ratio of approximately 0.5. The LDA usually underestimates the lattice constants. In our simulations, the external pressure is set to zero and the homogeneous strain is defined relative to the lattice constant value achieved by LDA calculations (the cubic lattice constant of bulk $BaTiO_3$ used in the effective Hamiltonian) instead of the experimental one. The simulation results at low temperatures are expected to converge to the first-principles calculations at zero temperature.

To comprehensively understand the inherent mechanism of the ferroelectric effect in the ultrathin $BaTiO_3$ film, we first investigate the polarization pattern of the films under compressive strains. The averaged out-of-plane polarization of a $20 \times 20 \times 8$ $BaTiO_3$ film is shown in figure 1(a) when the strain is -0.4%. Significant out-of-plane polarization can be clearly seen in this ultrathin (3.15 nm) film. Moreover, such polarization exhibits a periodic oscillation in the x–y plane which further indicates the existence of a unique polarization structure, the so-called '180° stripe domain structure' [26, 29].

Such stripe domains are also demonstrated in the spatial variation of the averaged polarization along the (110) direction (figure 1(b)), where u_z shows an oscillation which is similar to a cosine function, while u_x and u_y keep small values. Obviously, the peaks/valleys of u_z correspond to the centers of the stripe domain, while the nodal points correspond to the interfaces of two neighboring domains. Each stripe domain runs through the film along the growth direction, which is similar to the previous results of PZT films. [26]

Interestingly, it is found that the total out-of-plane polarization remains zero at any strain. This is consistent with the simulation results in quantum dots [19] and PZT films [26] where the normal component of polarization near the surface is suppressed by the vacuum. Therefore, such a 180° stripe domain is formed to minimize the energy of the depolarizing field under the constraint of the boundary condition that the film is surrounded by a vacuum without any surface charge screening. Similar 180° periodic stripe domains were also observed when the near-short-circuit electrical condition is used (i.e. the effect of surface charge screening is considered), as revealed theoretically by Lai *et al* very recently [14]. The above results indicate the stability of such a domain structure under realistic conditions.

To explore the mechanism of polarization, we further show the microstructure of local modes. The electrostatic interaction is an essential driving force in perovskite ferroelectrics [31]. In the $BaTiO_3$ thin films we studied, the long-range dipole–dipole interaction is expected to align the polarization vectors as 'head to end'. However, when we project the surface layer's polarization to the x–y plane (figure 2(a)), we found that the polarization vectors could be aligned as 'head to head' with each other. Such behavior is unusual. To explore the underlying physical mechanism, we plotted and analyzed the polarization projected on the $y = x$ plane. Interestingly, as shown in figure 2(b), a vortex polarization structure is observed in the $y = x$ plane. The clockwise and anticlockwise vortex appear alternately along the direction normal to the stripes. This vortex structure extends along the $(1\bar{1}0)$ direction as vortex stripes. The average effect of vortex structures directly results in the formation of 180° out-of-plane polarization stripe domains. The stripe domain walls are located at the centers of the vortex. Therefore each out-of-plane polarization domain does not superpose with the vortex stripe but strides across two neighboring vortex stripes.

The above vortex polarization structure originates from the balance between the long-range dipole–dipole interaction and short-range covalent interaction [20] and the effect of the free surface [32]. For the dipole–dipole interaction, the head to end alignment of polarization vectors is favorable in energy, while the constraint of the vacuum boundary condition and the absence of the screening effect tend to align the surface dipoles parallel to the surface to stabilize the dipole–dipole interaction. On the other hand, the existence of short-range covalent interaction requires that the dipoles change smoothly. Furthermore, in the internal parts of such films, due to the large compressive strain, the polarization tends to align out of plane. Obviously, the vortex polarization structures not only

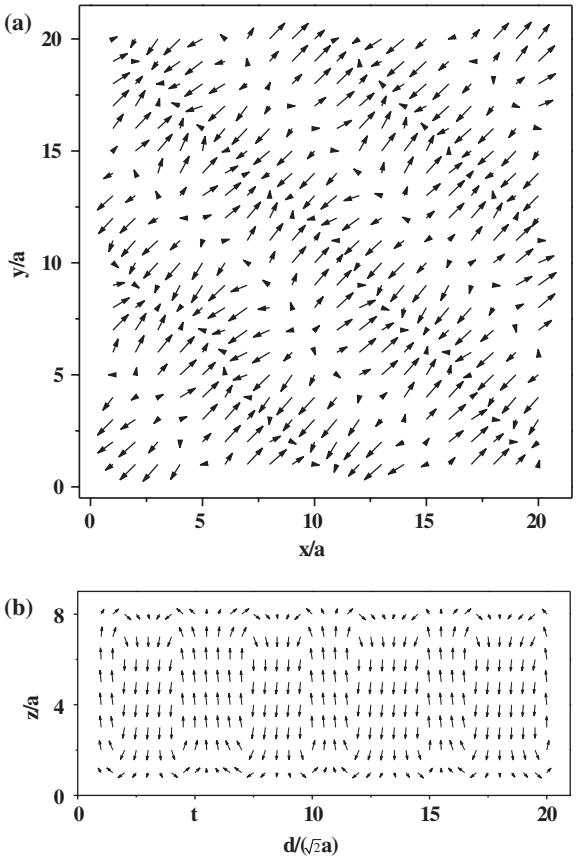

Figure 2. Local mode displacement $\mathbf{u}_i$ of a $20 \times 20 \times 8$ $BaTiO_3$ film with $T = 20$ K and $\eta = -0.4\%$. A vector arrow is used to virtualize the projection of $\mathbf{u}_i$ in the shown plane. (a) $\mathbf{u}_i$ of the cells in the surface plane. (b) $\mathbf{u}_i$ of the cells in the planes $x = y$ and $x = y + a$, which are projected on to the same plane.

fit for all the above analysis, but also effectively reduce the depolarization field by periodical arrangement.

In actual experimental systems and related devices, including ferroelectric capacitors and superlattices, the lattice constants (in the x–y plane) of ferroelectric films are determined by that of the substrate. It imposes an inherent strain effect on the films and consequently greatly changes the ferroelectric property of the films. So the strain is a substantial factor affecting the ferroelectric properties in such films. We have studied a series of $BaTiO_3$ film with different in-plane strains and calculated the averaged local mode (the supercell average of the in-plane components, u_x and u_y, and the average amplitude of the spatial variation of the out-of-plane component, u_z) and the homogeneous strain (η_H) as functions of both the strain and the temperature, which are used to identify the different phases. The resulting phase diagrams are presented in figure 3. It is found that the strain drastically changes the phase transition sequence. The phase diagram is divided into four parts with different phases (the notation is similar to that in [11–13] except that a superscript star ($*$) is added to indicate the existence of the stripe domains): (i) the paraelectric p phase at high temperatures with $u_x = u_y = u_z = 0$, where the symmetry of the system is lowered from cubic to tetragonal due to the clamping effect and the space

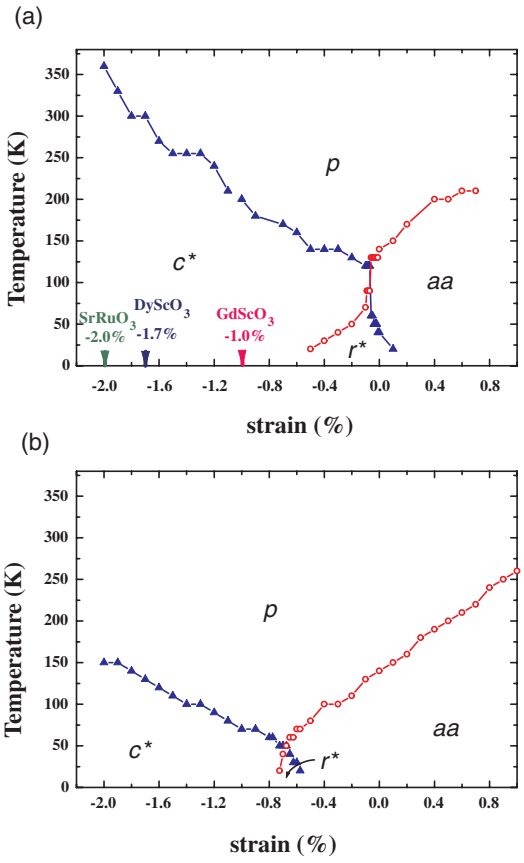

Figure 3. Phase diagrams of the (a) $15 \times 15 \times 6$ and (b) $15 \times 15 \times 4$ $BaTiO_3$ ultrathin films. The diagram is divided by a blue line (with solid triangles that separate $u_z = 0$ from $u_z \neq 0$) and a red line (with open circles that separate $u_x = u_y = 0$ from $u_x = u_y > 0$), resulting in four regions with different phases: ferroelectric c^* ($u_z > u_x = u_y = 0$), aa ($u_x = u_y > u_z = 0$), r^* ($u_x = u_y \neq 0$, $u_z \neq 0$), and paraelectric p ($u_x = u_y = u_z = 0$) phases. Domain structures form in both c^* and r^* phases, while the aa phase appears as a monodomain.

group is $P4/mmm$; (ii) the tetragonal ferroelectric c^* phase at high compressive strains, with (stripe domain) polarization $u_z > u_x = u_y = 0$ and the space group $P4mm$; (iii) the orthorhombic ferroelectric aa phase at high tensile strains, with in-plane polarization $u_x = u_y > u_z = 0$ and the space phase $Amm2$; (iv) the monoclinic ferroelectric r^* phase at low temperatures and low strains, with (stripe domain) polarization $u_x = u_y \neq 0$, $u_z \neq 0$, and the space group Cm. Due to the small size of the system, the possible adaptive structure [33] and medium averaged structure [34, 35] are not discussed here. In the c^* phase, the vortex stripes responsible for the 180° domains are observed. However, in the r^* phase, owing to $u_x = u_y \neq 0$, the stripe domains are not 180°, but approximately $2\arctan(u_z/\sqrt{{u_x}^2 + {u_y}^2})$, which depends on the strain and the temperature of the system. As the strain increases, the phase transition temperatures of the r^*–aa and c^*–p transitions decrease, whereas those of the c^*–r^* and p–aa transitions increase. This indicates that the compressive strain suppresses the in-plane polarization while supporting the out-of-plane polarization, thus driving the polarization to rotate from the in-plane to the normal direction [27]. The temperature region of the vortex stripe domain increases with the compressive strain. It is obvious that the compressive strain can stabilize the stripe domain. The film thickness has an obvious effect on the phase diagram of the ultrathin films. With decreasing film thickness, the Curie temperature decreases and the strain moves to more negative values. In spite of the changes with film thickness, both the structure of the phase diagram and the domain structure are well conserved in $BaTiO_3$ ultrathin films.

Our results are fully consistent with previous first-principles based calculations of the $BaTiO_3$ phase diagram under short-circuit conditions [12, 13], and comparable to the prediction of LGD theory [11]. Pertsev *et al* [11] first considered the temperature–strain phase diagram of $BaTiO_3$ based on an LGD theory using periodic boundary conditions, and predicted five phases: p, c, aa, ac (with polarization $p_x = p_z \neq 0$, $p_y = 0$), and r phases. The adoption of a first-principles-based approach resulted in a similar phase diagram except that the ac phase is now absent and the phase diagram is symmetric with respect to zero strain [12]. The inclusion of the surface effect into the first-principles-based calculations [13] confirmed the absence of the ac phase and the meeting of four phases at a single point, but the resulting phase diagram is not symmetric and the four-phase point is located at positive strain because the z-component of the polarization is particularly enhanced with respect to its other (x and y) components, especially close to the surfaces/interfaces. It was also indicated that a residual depolarizing field will shift the four-phase point towards more negative strain. In the current works, the extreme open-circuit condition with depolarization field is adopted to investigate its influence on the phase diagram of $BaTiO_3$ thin films. Figure 3 shows that the depolarization did not produce any new phases and the resulting phase diagram is very similar to that under short-circuit conditions. The main effect of the open-circuit conditions is to produce the z-direction polarization stripe domains instead of the monodomain in c^* and r^* phases (we use a superscript star ($*$) to emphasize the existence of stripe domains). So it is impossible to obtain a net out-of-plane polarization (e.g. monodomain) under the constraint of open-circuit boundary conditions because the out-of-plane polarization tends to align with alternative positive and negative orientations in order to reduce the depolarization energy. This characteristic of ultrathin films has been utilized to determine the critical thickness of ferroelectricity in $PbTiO_3$ ultrathin films recently [4]. On the whole, the influence of the depolarization field on the phase diagram of $BaTiO_3$ is relatively weak.

It is instructive to compare the $BaTiO_3$ phase diagram with that of $PbZr_{0.5}Ti_{0.5}O_3$ (PZT) thin films under the same open-circuit conditions. In fact, they are somewhat similar: our p, c^*, r^*, and aa phases correspond to the P, Sa, Sb, and O (M_c) phases in [18], which represent paraelectric phase, ferroelectric stripe phase without in-plane polarization, stripe phase with in-plane polarization, and monodomain phase with in-plane polarization, respectively. The similarity comes from the influence of the clamping effect and the depolarization field: since a polarization will elongate the lattice along the polarization direction, a tensile strain tends to retain the

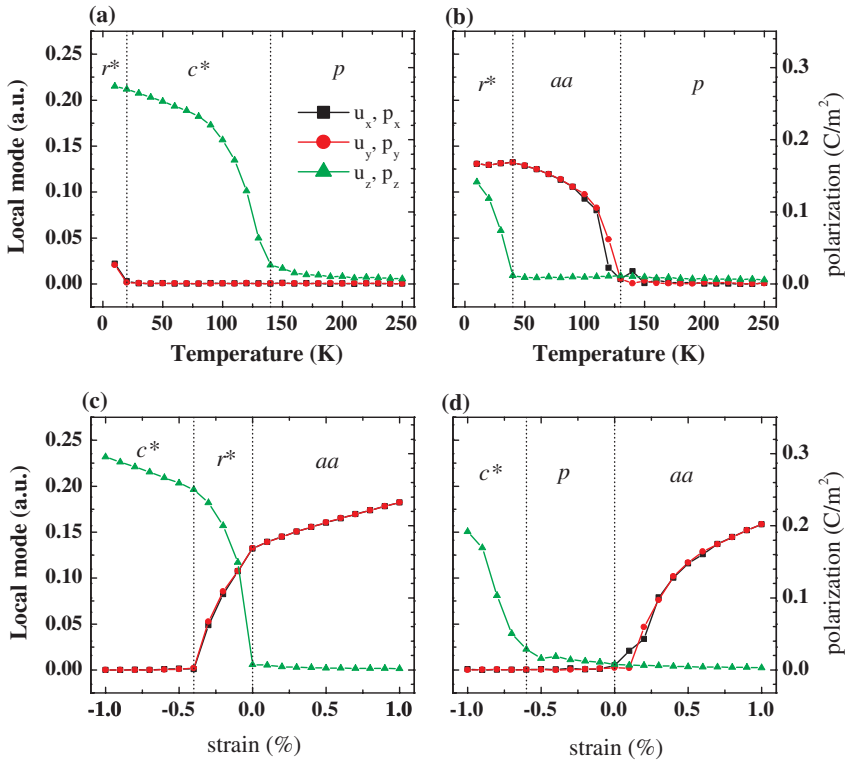

Figure 4. The supercell average of the in-plane local mode (u_x, u_y) and the average amplitude of the spatial variation of the out-of-plane local mode (u_z) of $15 \times 15 \times 6$ $BaTiO_3$ films as functions of the temperature at (a) $\eta = -0.5\%$ and (b) $\eta = 0$, and as functions of the strain at (c) $T = 40$ K and (d) $T = 150$ K. The right scales, which are proportional to each other, convert the local mode into the polarization.

polarization in-plane, while a compressive strain tends to drive the polarization out-of-plane, and then the depolarization field will turn the out-of-plane polarization into a stripe domain structure. A major difference between $BaTiO_3$ and PZT phase diagrams is that the in-plane polarization under tensile strains is along the x or y axis in PZT while it is along the (110) direction in $BaTiO_3$. This may be related to the intrinsic ferroelectricity in bulks. For bulk $BaTiO_3$, the low-temperature ferroelectric phases include tetragonal ($u_z > u_x = u_y = 0$), orthorhombic ($u_x = u_y > u_z = 0$), and rhombohedral ($u_x = u_y = u_z > 0$) phases, where the orthorhombic ferroelectric phase is compatible with the tensile strain of thin films and thus can be adopted in the phase diagram. For PZT, however, the bulk ferroelectric phase is either tetragonal or rhombohedral, so the polarization along the (110) direction is unfavorable in energy, and the in-plane polarization under tensile strains comes out to be along the x or y axis. Another difference is that, compared with PZT films, the $BaTiO_3$ films can be easily turned into the c^* phase with 180° stripe domain by imposing a relatively small strain (-0.3%). To achieve a stripe structure with out-of-plane polarization, the unfavorable domain boundary energy should be compensated by other favorite contributions such as chemical driving force and strain energy. $PbZr_{0.5}Ti_{0.5}O_3$ locates near the morphotropic phase boundary (MPB) and the energies of various phases are close to each other, so the paraelectric–ferroelectric chemical driving force is relatively small (which is the reason why an adoptive structure can be observed near MPB [36]), and a larger compressive strain is required to drive the polarization to be out-of-plane. The different ferroelectric lattice distortions may also play a role here since the tetragonal distortion of bulk PZT is almost twice that of $BaTiO_3$ (2% versus 1.1%). The c^* ferroelectric phase with an out-of-plane polarization is desired in many applications such as ferroelectric memory devices and quantum computing architecture, which was recently synthesized on an Si substrate [37]. In figure 3, we indicate the strains caused by substrates of $SrRuO_3$, $DyScO_3$, and $GdScO_3$, which will induce the c^* phase with higher ferroelectric stability.

Under different strain and temperature conditions, the $BaTiO_3$ thin films exhibit various sequences of phase transition (figure 4). When the strain is fixed as $\eta = -0.5\%$, the film exhibits a r^* phase at low temperature, and it undergoes two phase transitions when the temperature increases: r^*–c^*, and c^*–p transitions. When $\eta = 0$, at low temperature the film also exhibits a r^* phase. However, two different phase transitions occur in this system with increasing temperature: r^*–aa and aa–p transitions. When the temperature is fixed at $T = 40$ K, as the strain increases, the film subsequently undergoes c^*–r^* and r^*–aa phase transitions. While at a higher temperature $T = 150$ K, paraelectric phase exists when the strain is close to zero, so the film undergoes c^*–p and p–aa phase transitions with increasing strain. Figure 3 clearly indicates that the in-plane polarizations u_x and u_y stay the same under any conditions, which decrease with increasing the (compressive) strain and disappear when the strain arrives at a critical value.

In this paper the extreme open-circuit boundary condition has been adopted as an extreme approach. An obvious

concern is whether this condition is realistic. In experimental systems with ferroelectric thin films grown on insulating substrates, because the finite bulk conductivity and the metal-like surface conductivity of the ferroelectric film are small, the screening of the surface polarization charge will require a time far larger than the time of the switching of the polarization. Therefore, the polarization charges are probably screened incompletely, while the ferroelectric phase will form in domains of alternating polarity to reduce the electric field energy arising from the polarization (the depolarizing field). In fact, many works indicate that the polarization charge cannot be perfectly screened by free charge in thin films. For example, the 180° stripe domain has been experimentally observed in $PbTiO_3$ ferroelectric thin films [4, 38], indicating the validity of the open-circuit condition in this case. Dunn *et al* showed that the surface spontaneous depolarization field of ferroelectrics can be used to direct the assembly of virus particles [39]. Therefore, studies under various conditions (short-circuit, open-circuit, and partly charge screening conditions) can provide a comprehensive understanding of ferroelectric thin films.

In thin films, the epitaxial strain imposed by the substrate is usually recognized as the major factor in determining the structure and property differences with the bulks. Other factors, such as the chemical activity of the available substrates, also contribute to the difference between ferroelectric properties of thin films and bulk [40–42]. For example, the atomic bonding in a $BaTiO_3$/Fe system will induce a ferroelectricity–magnetism coupling [40]. The chemical activity of available substrates is often diverse, which can be utilized in experiments. In our study, the substrate is mimicked just by imposing in-plane strains while the influences of other factors are not pursued. In other words, an inert substrate is assumed to be modeled in the simulations.

In summary, the strain–temperature phase diagrams of $BaTiO_3$ ultrathin films under open-circuit conditions have been obtained using first-principles based simulations. The phase diagram is similar to that under short-circuit conditions, while 180° stripe domain and vortex polarization patterns are observed in the phases with out-of-plane polarization (component) under compressive strains. The mechanism of such a polarization structure is related to a balance between long-range and short-range interactions, and also depends on specific boundary conditions. The strain is found to be crucial for such a polarization structure since it supports the out-of-plane polarization but suppresses the in-plane polarization.

Acknowledgments

This work was supported by the National Natural Science Foundation of China (Grant Nos. 10325415 and 50432030) and the Ministry of Science and Technology of China (Grant No. 2006CB605105).

References

[1] Setter N *et al* 2006 *J. Appl. Phys.* **100** 051606
[2] Wang Y, Cheng Y L, Cheng K C, Chan H L W, Choy C L and Liu Z R 2004 *Appl. Phys. Lett.* **85** 1580
[3] Tyunina M, Levoska J and Jaakola I 2006 *Phys. Rev.* B **74** 104112
[4] Fong D D, Stephenson G B, Streiffer S K, Eastman J A, Auciello O, Fuoss P H and Thompson C 2004 *Science* **304** 1650
[5] Zheng H *et al* 2004 *Science* **303** 661
[6] Buchanan R C (ed) 1997 *Ceramic Materials for Electronics* (New York: Dekker)
[7] Ahn C H, Rabe K M and Triscone J M 2004 *Science* **303** 488
[8] Setter N (ed) 2005 *Electroceramic-Based MEMS* (New York: Springer)
[9] Tenne D A *et al* 2006 *Science* **313** 1614
[10] Choi K J *et al* 2004 *Science* **306** 1005
[11] Pertsev N A, Zembilgotov A G and Tagantsev A K 1998 *Phys. Rev. Lett.* **80** 1988
[12] Dieguez O, Tinte S, Antons A, Bungaro C, Neaton J B, Rabe K M and Vanderbilt D 2004 *Phys. Rev.* B **69** 212101
[13] Lai B K, Kornev I A, Bellaiche L and Salamo G J 2005 *Appl. Phys. Lett.* **86** 132904
[14] Lai B K, Ponomareva I, Kornev I A, Bellaiche L and Salamo G J 2007 *Phys. Rev.* B **75** 085412
[15] Junquera J and Ghosez P 2003 *Nature* **422** 506
[16] Kim D K, Jo J Y, Kim Y S, Chang Y J, Lee J S, Yoon J G, Song T K and Noh T W 2005 *Phys. Rev. Lett.* **95** 237602
[17] Kornev I, Fu H and Bellaiche L 2004 *Phys. Rev. Lett.* **93** 196104
[18] Wu Z Q, Huang N D, Wu J, Duan W H and Gu B L 2005 *Appl. Phys. Lett.* **86** 202903
[19] Fu H and Bellaiche L 2003 *Phys. Rev. Lett.* **91** 257601
[20] Wu Z Q, Huang N D, Liu Z R, Wu J, Duan W H and Gu B L 2007 *J. Appl. Phys.* **101** 014112
[21] Bühlmann S, Colla E and Muralt P 2005 *Phys. Rev.* B **72** 214120
[22] Duan W H and Liu Z R 2006 *Curr. Opin. Solid State Mater. Sci.* **10** 40 and references therein
[23] Resta R 2003 *Modelling Simul. Mater. Sci. Eng.* **11** R69
[24] Zhong W, Vanderbilt D and Rabe K M 1995 *Phys. Rev.* B **52** 6301
[25] Bellaiche L, Garcia A and Vanderbilt D 2000 *Phys. Rev. Lett.* **84** 5427
[26] Wu Z Q, Huang N D, Liu Z R, Wu J, Duan W H, Gu B L and Zhang X W 2004 *Phys. Rev.* B. **70** 104108
[27] Huang N D, Liu Z R, Wu Z Q, Wu J, Duan W H, Gu B L and Zhang X W 2003 *Phys. Rev. Lett.* **91** 067602
[28] Shin Y H, Cooper V R, Grinberg I and Rappe A M 2005 *Phys. Rev.* B **71** 054104
[29] Tinte S and Stachiotti M G 2001 *Phys. Rev.* B. **64** 235403
[30] Bródka A and Grzybowski A 2002 *J. Chem. Phys.* **117** 8208
[31] Zhang X W, Wang Q and Gu B L 1991 *J. Am. Ceram. Soc.* **74** 2846
[32] Fu L, Yaschenko E, Resca L and Resta R 1999 *Phys. Rev.* B **60** 2697
[33] Jin Y M, Wang Y U, Khachaturyan A G, Li J F and Viehland D 2003 *Phys. Rev. Lett.* **91** 197601
[34] Glazer A M, Thomas P A, Baba-Kishi K Z, Pang G K H and Tai C W 2004 *Phys. Rev.* B **70** 184123
[35] Bokov A A and Ye Z-G 2006 *J. Mater. Sci.* **41** 31
[36] Wang H, Zhu J, Lu N, Bokov A A, Ye Z G and Zhang X W 2006 *Appl. Phys. Lett.* **89** 042908
[37] Vaithyanathan V *et al* 2006 *J. Appl. Phys.* **100** 024108
[38] Streiffer S K, Eastman J A, Fong D D, Thompson C, Munkholm A, Murty M V R, Auciello O, Bai G R and Stephenson G B 2002 *Phys. Rev. Lett.* **89** 067601
[39] Dunn S, Cullen D, Abad-Garcia E, Bertoni C, Carter R, Howorth D and Whatmore R W 2004 *Appl. Phys. Lett.* **85** 3537
[40] Duan C G, Jaswal S S and Tsymbal E Y 2006 *Phys. Rev. Lett.* **97** 047201
[41] Dawber M, Chandra P, Littlewood P B and Scott J F 2003 *J. Phys.: Condens. Matter* **15** L393
[42] Tinte S and Stachiotti M G 2001 *Phys. Rev.* B **64** 235403